IEEE Access
Multidisciplinary | Rapid Review | Open Access Journal

Received January 23, 2019, accepted February 21, 2019, date of publication March 19, 2019, date of current version June 27, 2019.

Digital Object Identifier 10.1109/ACCESS.2019.2903123

Automatic 3D Registration of CT-MR Head and Neck Images With Surface Matching

QIN CHU[1], YINWEI ZHAN[1], FANQING GUO[2,3], MENGCHUN SONG[4], AND RONGQIAN YANG[2,5,6]

[1]Interactive and Visual Informatics, School of Computer Science and Technology, Guangdong University of Technology, Guangzhou 510006, China
[2]School of Medicine, Yale University, New Haven, CT 06520, USA
[3]Department of Therapeutic Radiology, Yale-New Haven Hospital, New Haven, CT 06520, USA
[4]Guangdong Medical Devices Quality Surveillance and Test Institute, Guangzhou 510663, China
[5]Department of Biomedical Engineering, South China University of Technology, Guangzhou 510006, China
[6]Guangdong Engineering Technology Research Center for Translational Medicine of Mental Disorders, Guangzhou 51006, China

Corresponding author: Rongqian Yang (yangrongqian@gmail.com)

This work was supported in part by the National Natural Scientific Foundation of China under Grant 81671788, in part by the Guangdong Provincial Science and Technology Program under Grant 2016A020220006, Grant 2017B020210008, and Grant 2017B010110015, in part by the Fundamental Research Funds for Central Universities under Grant 2017ZD082, in part by the Guangzhou Science and Technology Program under Grant 201704020228, and in part by the Chinese Scholarship Fund under Grant 201806155010.

ABSTRACT Radiotherapy is a major treatment for head and neck cancer. Currently, computed tomography (CT) is utilized to delineate the target area and make radiotherapy plans. Compared with CT images, magnetic resonance (MR) images have excellent soft tissue contrast, which can distinguish normal surrounding tissues. It is necessary to register MR and CT images since it helps physicists to improve the accuracy of radiotherapy plans. Most of the current registrations require manual intervention to select regions of interest, which increases the workload of doctors and the time of registration to a certain extent. In this paper, an automatic registration method is proposed to delineate the regions of interest. Herein, surface meshes are extracted from the CT and MR images and utilized to perform the surface matching, then the regions of interest are extracted automatically by calculating the overlapped regions between the surface mesh of the surface-aligned MR images and CT images. Furthermore, a multi-level resolution registration mechanism is utilized to improve the registration speed. Surface matching is performed using low-resolution images to obtain transformation parameters as initial parameters for rigid registration followed by deformable registration. The experiments demonstrate that our proposed method performs better in the registration speed and accuracy over the conventional methods of delineating regions of interest manually.

INDEX TERMS Automatic extraction, image registration, mutual information, surface matching.

I. INTRODUCTION

Nasopharyngeal carcinoma is a common head and neck cancer in southern China. In 2017, there were 5,609 new cases of nasopharyngeal carcinoma. Radiation therapy is one of the most commonly used treatments nasopharyngeal carcinoma. The goal of radiation therapy is to adequately illuminate the tumor area while reducing the dose of surrounding healthy tissues. Most modern strategies, such as image guided radiation therapy (IGRT) and intensity modulated radiation therapy (IMRT), can accurately deliver high doses to the clinical target volume (CTV), providing a progressive approach to more focused treatment; here CTV is based on computed tomography (CT) [1], [2]. However, CT images cannot provide high contrast between healthy tissue and tumor tissue so that the healthy tissue surrounding the tumor is likely to be exposed to excessive radiation. In contrast to CT images, magnetic resonance (MR) images provide a rich soft tissue contrast so that can be taken as a reference for head and neck tumor delineation [3]–[6]. In order to improve the effectiveness of radiotherapy, it is necessary for radiotherapy plans to be combined with MR images.

In general, there are three methods for MR-based radiotherapy planning. One is based on MR-only planning, which is proposed to generate pseudo-CT from MR 3D images [7], [8], providing electron density information, but pseudo CT and CT images are still fundamentally different. one is based on image synthesis for registration,

The associate editor coordinating the review of this manuscript and approving it for publication was György Eigner.

which proposed using a structured random forest and auto-context model to synthesize CT from MR and synthesize MR from CT. However, it may not be so accurate in the learning process, resulting in differences between synthesis CT and CT in essence. Another is a registration method to register MR images in planned CT scans in order to improve targeting accuracy [9], [10]. By using registration method, the first step is to extract regions of interest (ROI). McLaughlin *et al.* [11] proved that using mutual information (MI) within the ROI on both MR and CT images can reduce the effects of anatomical deformation. Their method obtains good results, while requires manual intervention to select the ROI. Some recent works with good registration results can be referred to [12], [13]. All these methods select the ROI manually, which makes the registration operation more complicated. At the same time, the size of the ROI is of randomness because of manual delineation, which may result in unreliable registration results in practice.

To avoid position shift of the patient, a trick of rigid registration [14], [15] is then introduced by letting the patient wear a specific fixed mask and headrest during acquisition of CT and MR images. However, imperfections of the fixed mask result in non-rigid deformation between the CT and MR images; a solution of this problem found in [16], [17] is by deformable registration between CT and MR images in head and neck region. In [16] the alignment of 4 patients was evaluated using unspecified anatomic landmarks, and in [17] the registration parameters were optimized with respect to the best accuracy obtained over the entire dataset of 12 patients. The key point in these works is that it is necessary to extract the ROI for whether rigid or deformable registration.

To further better the case, in this paper, we propose an automated registration method to extract the ROI automatically. In particular, surface meshes are extracted from the CT and MR images and is utilized to perform surface matching for aligning MR with CT spatially. In addition, multi-resolution rigid registration is adopted to improve the performance of MR-CT image registrations in head and neck region. Furthermore, to decrease non-rigid deformation in the head and neck region, the deformable registration is utilized after rigid registration. Our strategy can improve the registration accuracy, simplify the registration procedure, and reduce the error caused by manual intervention.

The rest of this paper is organized as follows. The proposed method is introduced in Section II, followed by extensive experiments conducted in Section III. In Section IV, the result and discussion are analyzed. Finally, we conclude this paper in Section V.

II. METHOD

Our automatic registration method consists of three parts. The first part is surface matching that includes images preprocessing, surface meshes extraction, obtaining the overlapped region by matching, and getting the ROI. The second part is rigid and deformable registration that utilizes the ROI generated in the first part as the input of the rigid registration followed by the deformable registration. The third part is to fuse the CT images and registered MR images.

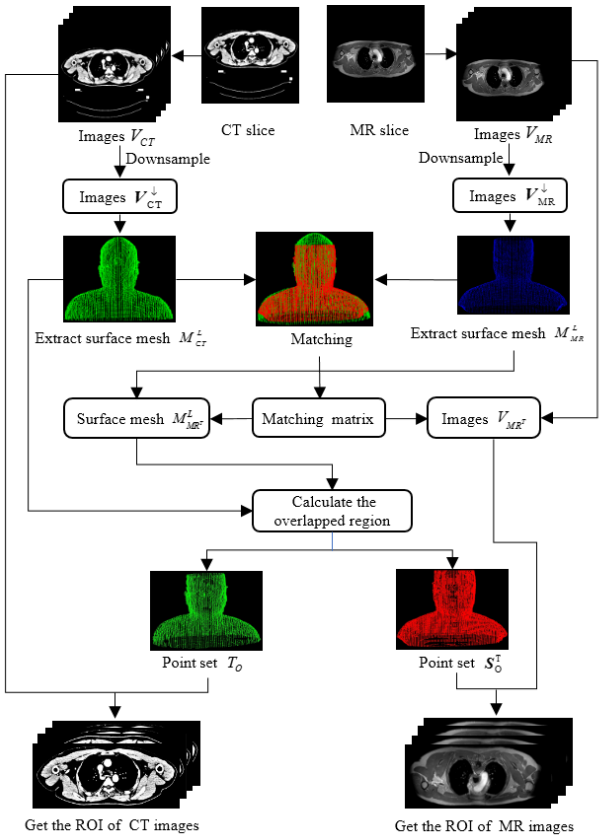

FIGURE 1. The flowchart for automatically extracting ROI. Surface matching is performed on surface meshes M_{CT}^{L} and M_{MR}^{L}, M_{MR}^{L} is resampled by using the matching matrix to obtain $M_{MR^T}^{L}$, and the overlapping area of M_{CT}^{L} and $M_{MR^T}^{L}$ is calculated to obtain the ROI.

A. SURFACE MATCHING

Given a set of CT images V_{CT} of head and neck region of a patient and the corresponding MR images V_{MR}, the goal of the surface matching is to generate the ROI of the CT and MR images. It mainly includes downsampling images, extracting the surface meshes for matching, and resampling the meshes and images by matching matrix; see Fig. 1.

1) IMAGE PREPROCESSING

Before registration, the images V_{CT} and V_{MR} are smoothed with anisotropic diffusion filters, which was based on the heat conduction (diffusion) equation. In higher gradient regions, such as region boundaries, the diffusion effects to become less noticeable, thus remains sharp of the region boundaries of the image. In order to speed up the registration process, the smoothed images are then downsampled by a factor of 2^F along the x-axis and y-axis, while the z-axis direction remains unchanged. Let $V_{CT}^{\downarrow}$ and $V_{MR}^{\downarrow}$ be the downsampled versions of V_{CT} and V_{MR}, respectively.

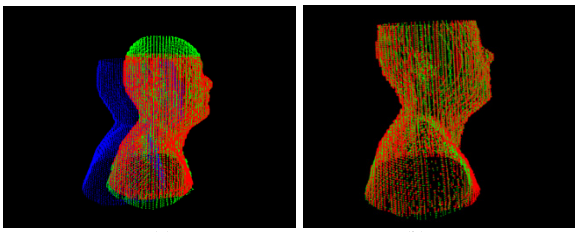

FIGURE 2. Get overlapped regions: (a) The green, blue, and red one repres- ent T, S, and S^T, respectively; (b) Overlapped regions of two point sets. The green, red one are the T_o and S_o^T, respectively.

2) EXTRACT SURFACE MESHES

Surface meshes M_{CT} and M_{MR} are extracted from the $V_{CT}^{\downarrow}$ and $V_{MR}^{\downarrow}$ with Marching Cubes (MC) algorithm [18], which creates triangle models of constant density surfaces from 3D medical data and uses a divide-and-conquer approach to locate the surface in a logical cube created from eight pixels; four each from two adjacent slices to generate inter-slice connectivity. However, M_{CT} and M_{MR} may have multiple connected object regions, so the connected region of the largest number of points is taken to be the accurate surface meshes M_{CT}^L and M_{MR}^L.

3) GET OVERLAPPED REGIONS

It should be noticed that the parts scanned with CT and MR may not be identical. So the corresponding images along z direction may have uneven slices, while the two sets of slices may have different resolutions along the x and y directions. Therefore, to match surface meshes is to fundamentally find the counterparts of the both sets of slices.

Here, we use Iterative Closest Point (ICP) algorithm [19] to realize surface matching on M_{CT}^L and M_{MR}^L via

$$T_{MR\to CT}, M_{MR^T}^L, \varepsilon = ICP(M_{CT}^L, M_{MR}^L), \tag{1}$$

where $T_{MR\to CT}$ is the matrix that transforms the counterpart of M_{MR}^L to that of M_{CT}^L, $M_{MR^T}^L = T_{MR\to CT}(M_{MR}^L)$, and ε represents the error of surface matching. Take $V_{MR^T} = T_{MR\to CT}(V_{MR})$ and denote T, S, and S^T as the sets of vertices of the surface meshes M_{CT}^L, M_{MR}^L, and $M_{MR^T}^L$, respectively. After matching, the point set T is assembled with overlaps of the point set S^T; see Fig. 2 (a).

Let C be the minimum cuboid containing both T and S^T. Now we divide C into n equal cubes $c_1, c_2, \ldots, c_n$ of side length $P = 2\varepsilon$. Denote by V_C the volume of C. Then, the number of the small cubes can be performed as $n = V_C/P^3$. We keep all the small cubes of indices $J \subset \{1, \ldots, n\}$ that satisfy $c_i \cap T \neq \emptyset$ and $c_i \cap S^T \neq \emptyset$, for $i \in J$. Then, the overlapped regions of T and S^T are obtained as $T_o = \cup_{i\in J} c_i \cap T$, and $S_o^T = \cup_{i\in J} c_i \cap S^T$; see Fig. 2 (b).

4) GET THE CORRESPONDING OVERLAPPED REGIONS IN 3D IMAGES

In order to obtain the corresponding image region based on T_o and S_o^T, surface reconstruction is performed on S_o^T to get

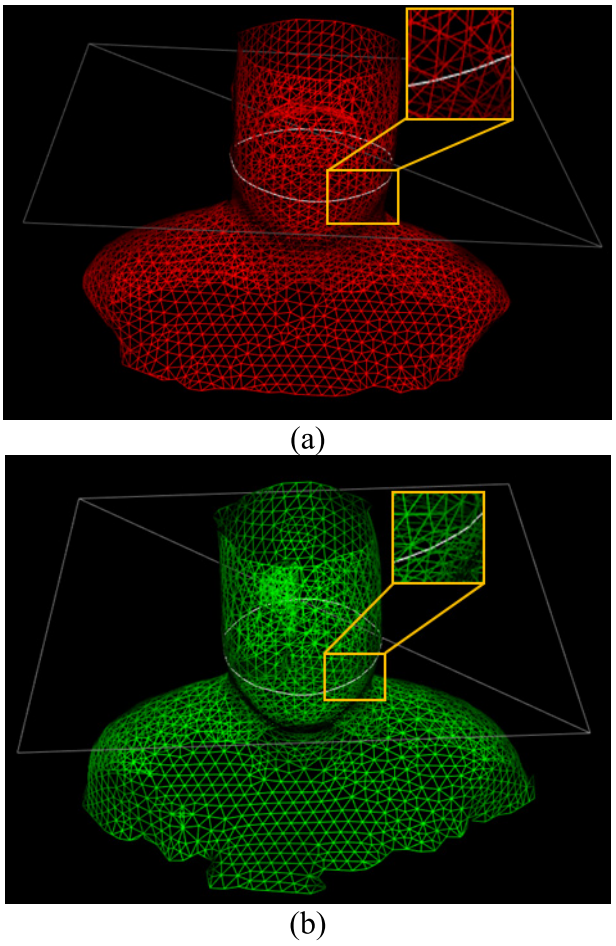

FIGURE 3. The surface model intersects the plane to get the intersection. (a), (b) are the intersection of the surface reconstruction model of the MR images, CT images, respectively.

$M_{S_o^T}$ [20], then, V_{MR^T} is downsampled to the same resolution as $V_{CT}^{\downarrow}$ assumed as $V_{MR^T}^{\downarrow}$, with the pixel spacing dx, dy, and dz in the x-axis, y-axis, and z-axis directions. Let N_z be the number of slices, and N_x and N_y be the length and width of a slice.

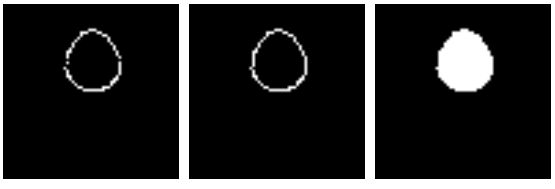

FIGURE 4. Binary image of the ROI: (a) Set the pixel value of the intersection to 255. (b) Connect the intersection end to end. (c) Fill holes.

Consider the plane G_z passing $(0, 0, z)$ and perpendicular to the z-axis $V_{MR^T}^{\downarrow}$, repeat the operation for $V_{CT}^{\downarrow}$, the result is shown in Fig. 3. Then take the intersection of G_z with $M_{S_o^T}$, set the pixel values of the intersection points as 255. Connect these points sequentially and fill the hole. The resulted slice can be regarded as a binary image I_z; see Fig. 4 (c).

(a) (b) (c)

FIGURE 5. Get the ROI of the original image. (a) Upsample I_z and then use the closing operation in morphology to process. (b) Upsampled I_z corresponds to the same resolution CT image. (c) Obtain the final ROI.

Now upsample I_z to the same resolution as the corresponding slice in V_{CT} and perform the closing operation in morphology to eliminate the edge glitches of I_z. It results in a hole-filling image B_z of smooth contours as illustrated in Fig. 5 (a), which can be also regarded as a set that indicates the domain of the ROI in slice V_z. The segment of V_z on B_z is illustrated in Fig.5 (c).

Repeat the above operations for all the slices, and finally obtain the ROI

$$V_{CT}^{R} = \cup_{1 \le z \le N_z} B_z \ of \ V_{CT}. \tag{2}$$

Similarly, we can obtain the ROI V_{MR}^{R} of V_{MR^T} by following the above operations.

B. RIGID AND DEFORMABLE REGISTRATION

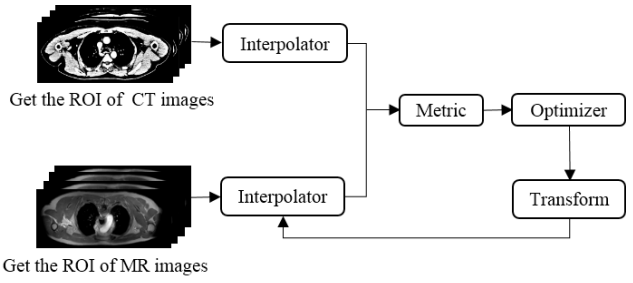

FIGURE 6. Workflow for the MR to CT images registration.

In order to speed up the registration process, lower resolution images V_{CT}^{R} and V_{MR}^{R} are utilized as the input of the rigid registration in Fig. 6 and $T_{MR \to CT}$ is utilized as the initial parameters. The rigid registration can be denoted as

$$T_{MR^R \to CT^R}, V_{MR'}^{R} = T_1(V_{CT}^{R}, V_{MR}^{R}, T_{MR \to CT}), \tag{3}$$

where T_1 is the operation of rigid registration, $T_{MR^R \to CT^R}$ is the matrix that transforms V_{MR}^{R} to V_{CT}^{R}, and $V_{MR'}^{R} = T_{MR^R \to CT^R}(V_{MR}^{R})$. Let $V_{MR^T}^{1} = T_{MR^R \to CT^R}(V_{MR^T})$.

However, there are still non-rigid deformation in the head and neck, so $V_{MR'}^{R}$ is taken as the input of deformable registration, it can be denoted as

$$D_{MR^R \to CT^R}, V_{MR''}^{R} = T_2(V_{CT}^{R}, V_{MR'}^{R}), \tag{4}$$

where T_2 is the operation of deformable registration, $D_{MR^R \to CT^R}$ deforms $V_{MR'}^{R}$ to V_{CT}^{R}, and $V_{MR''}^{R} = D_{MR^R \to CT^R}(V_{MR'}^{R})$. Let $V_{MR^T}^{2} = D_{MR^R \to CT^R}(V_{MR^T}^{1})$.

C. IMAGE FUSION

After registration, image fusion is performed on V_{CT} and $V_{MR^T}^{2}$ to improve the image quality and evaluate the registration effect. For suitable weights a and b, the fused image is

$$V_F = aV_{CT} + bV_{MR^T}^{2}. \tag{5}$$

III. EXPERIMENTS

A. DATASET

In order to evaluate the proposed method, we collected CT and MR image data of 50 nasopharyngeal carcinoma patients, including 6,100 CT images and 5,000 MR images. In our experiments, the CT1c and T1c images are chosen for registration.

More specifically, CT and MR images are acquired from the same patients with nasopharyngeal carcinoma for radiotherapy planning. CT images are acquired using a Siemens scanner (Somatom Definition as Germany), with $512 \times 512 \times 122$ voxels of $0.977 \times 0.977 \times 3\ mm^3$, and MR images are acquired using Philips Medical Systems, with $720 \times 720 \times 100$ voxels of $0.694 \times 0.694 \times 3\ mm^3$. In addition, all patients wear a patient-specific immobilization mask and headrest during the acquisition under the treatment position.

B. EVALUATION CRITERIA

The evaluation criteria include the mutual information (MI) [21]–[23] that ranges from 0 to 1; higher value of MI indicates better performance. In particular, through gradient descent optimization method of regular step, MI value is calculated per iteration. When the step size is less than the preset minimum step size, or the number of iterations is greater than the preset maximum iteration number, the iteration is stopped. Then, MI value is recorded.

C. INFLUENCE OF DIFFERENT RESOLUTIONS

In order to evaluate the influence of different resolutions on our method, images are downsampled by a factor 2^F. Here, the same optimizer parameters are set (the learning rate $\lambda_L = 0.2$; the minimum step size of the optimizer $\lambda_S = 0.001$) and images are downsampled in the x-axis and y-axis direction, and the z-axis direction remains unchanged in the comparison experiments. In addition, the center transform module is utilized to initialize the transform center and translation, and the center of rotation is approximately $(0, -257.1, 8.4)$, and the initial translation is approximately $(-16, 176, -32)$.

As shown in Table 1, low resolution images are used in the proposed approach reducing the computation time, and improving the accuracy of registration in some extent. When images are downsampled by $1/8(F = 3)$, MI_{Mean} is much higher than that by $1/2(F = 1)$. When images are downsampled by $1/16(F = 4)$, MI_{Mean} is only about 0.5, because images lose too much information.

D. EFFECTIVENESS OF OUR PROPOSED APPROACH

In order to verify the effectiveness of our method, we set up three sets of experiments based on different resolutions.

TABLE 1. Experimental results utilizing the proposed method with different samplings. MI_{Mean} and $Time_{Mean}$ are the average of MI and time for 50 patients. MI_{Stdev} and $Time_{Stdev}$ are the standard deviation of MI and time for 50 patients.

F	XY downsampling		Z downsampling		MI_{Mean}	MI_{Stdev}	$Time_{Mean}$(s)	$Time_{Stdev}$(s)
	CT	MR	CT	MR				
4	16:1	16:1	1:1	1:1	0.514	0.134	17.832	4.335
3	8:1	8:1	1:1	1:1	0.759	0.083	35.591	3.972
2	4:1	4:1	1:1	1:1	0.643	0.096	127.438	10.318
1	2:1	2:1	1:1	1:1	0.603	0.097	513.807	33.859
0	1:1	1:1	1:1	1:1	0.522	0.124	1835.12	35.246

TABLE 2. Experimental results using the proposed method compared with Mattes mutual information(Mattes.MI) without delineating ROI and with delineating ROI manually.

F	Method	MI_{Mean}	MI_{Stdev}	$Time_{Mean}$(s)	$Time_{Stdev}$(s)
3	Without ROI+Mattes.MI	0.451	0.091	170.53	4.216
	ROI manually+Mattes.MI	0.714	0.127	40.69	7.546
	Proposed	0.759	0.083	35.591	3.972
2	Without ROI+Mattes.MI	0.467	0.098	621.61	12.134
	ROI manually+Mattes.MI	0.602	0.142	137.57	17.229
	Proposed	0.643	0.096	127.438	10.318
1	Without ROI+Mattes.MI	0.462	0.101	2501.86	35.65
	ROI manually+Mattes.MI	0.581	0.153	532.19	39.874
	Proposed	0.603	0.097	513.807	33.859

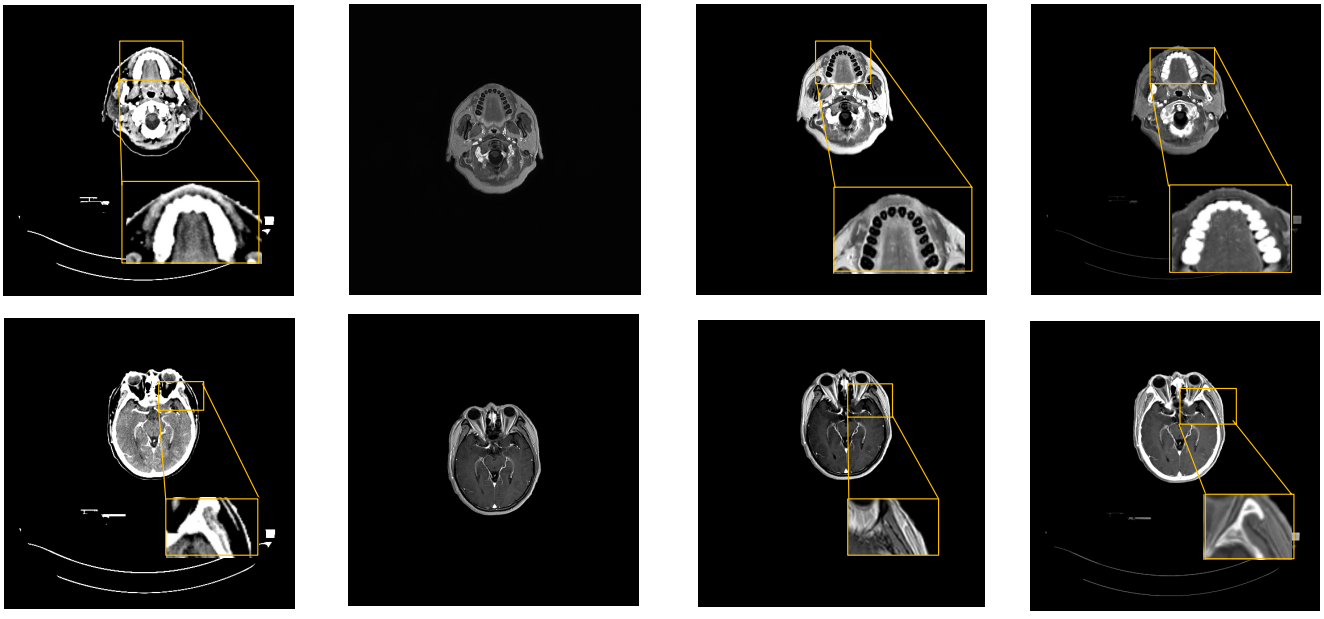

(a) (b) (c) (d)

FIGURE 7. Image fusion of registered MR and CT image. (a) Original CT image. (b) Original MR image. (c) Registered MR image. (d) Fusion of the original CT image and registered MR image.

The first group uses the Mattes mutual information with delineating the ROI manually for registration. The second group uses Mattes mutual information without delineating the ROI. The third group is to automatically delineate the ROI using the method shown in Fig.1, and then performs the rigid and deformable registrations shown in equations (3) and (4) based on the ROI. The results of the experiment shown in Table 2.

It can be seen from Table 2 that without delineating ROI, MI_{Mean} is only about 0.4 since that in a limited number of

iterations, iterating through the entire image to calculate the MI value is time consuming and does not get the optimal value of MI. Table 2 shows that manual delineation of ROI is a little slower than our method, but it cannot process large amounts of data, and may cause some noise when delineating it manually. MI_{stdev} of the manual delineation ROI is larger than that of the automatic delineation ROI using our method, because the size of the delineation area manually is different which affects the registration result. In summary, our method is more accurate than other methods in the registration of the test data. In addition, the time-consuming of our method is reduce in a certain extent and the registration can be made more flexible since ROI can be automatically extracted, which reduces the impact of human operations on registration.

IV. RESULT VISUALIZATION

As shown in Fig. 7, one slice of CT images is sampled in Fig. 7 (a), and its corresponding slice of MR images in Fig. 7 (b). The registered MR image is in Fig. 7 (c), and the fusion result from the registered MR image and CT image is in Fig. 7 (d). It can be seen from Fig. 7 (a) and Fig. 7 (c) that the registered MR image is basically consistent with the CT image. In Fig. 7 (d), the registered MR image and CT image can be fused to compensate for the poor contrast of soft tissue to CT image. In particular, in the first row of images, CT image is obvious for the tooth profile, but the peripheral soft tissue is very blurred. In registered MR image, although the tooth profile cannot be seen, the peripheral soft tissue is very rich. By fusing CT and registered MR image, the tooth profile and peripheral soft tissue can be seen simultaneously. In the second row of images, CT image is obvious for the periorbital bones, but lacking of soft tissue information. In registered MR image, no bone information can be seen, but the soft tissue around the orbit can be clearly seen. By fusing CT and registered MR image, the bone and soft tissue parts of the orbit can be seen simultaneously, which demonstrate the effectiveness of our proposed method.

V. CONCLUSIONS AND FUTURE WORK

In this study, a method is proposed for extracting the ROI to register MR and CT images automatically. Our method performs surface matching on the surface mesh, which spatially align MR images with CT images and obtain the overlapped region of the two images as the input of the registration. The key innovation is to automatically extract the ROI reducing artificial interference. At the same time, multi-resolution registration is utilized. First, low-resolution images are utilized for registration, and then transform parameters are obtained to initialize the registration parameters of high-resolution images. The result demonstrates that our method can improve the accuracy of registration and reduce the registration time in a certain extent. Although our algorithm has better results in the head and neck region, it has not been tested in other parts of the body, such as the lungs and abdomen. In the future, we will be devoted to register other parts with the proposed method and will try to use deep learning for head and neck registration, because it does not need to extract the ROI when registering, which simplifies the registration process, but it needs a lot of head and neck data to train to get better results, this will be our work in the next step.

REFERENCES

[1] P. M. Evans, "Anatomical imaging for radiotherapy," *Phys. Med. Biol.*, vol. 53, no. 12, p. R151, 2008.

[2] M. Paulides *et al.*, "The clinical feasibility of deep hyperthermia treatment in the head and neck: New challenges for positioning and temperature measurement," *Phys. Med. Biol.*, vol. 55, no. 9, p. 2465, 2010.

[3] L. M. Toonkel, K. Soila, D. Gilbert, and J. Sheldon, "MRI assisted treatment planning for radiation therapy of the head and neck," *Magn. Reson. Imag.*, vol. 6, no. 3, pp. 315–319, 1988.

[4] M. Ahmed *et al.*, "The value of magnetic resonance imaging in target volume delineation of base of tongue tumours–a study using flexible surface coils," *Radiotherapy Oncol.*, vol. 94, no. 2, pp. 161–167, 2010.

[5] A. R. Gordon *et al.*, "Intraobserver variability in the MR determination of tumor volume in squamous cell carcinoma of the pharynx," *Amer. J. Neuroradiol.*, vol. 25, no. 6, pp. 1092–1098, 2004.

[6] C. R. Rasch *et al.*, "Decreased 3D observer variation with matched CT-MRI, for target delineation in nasopharynx cancer," *Radiat. Oncol.*, vol. 5, no. 1, p. 21, 2010.

[7] J. A. Dowling *et al.*, "An atlas-based electron density mapping method for magnetic resonance imaging (MRI)-alone treatment planning and adaptive MRI-based prostate radiation therapy," *Int. J. Radiat. Oncol. Biol. Phys.*, vol. 83, no. 1, pp. e5–e11, 2012.

[8] S.-H. Hsu, Y. Cao, K. Huang, M. Feng, and J. M. Balter, "Investigation of a method for generating synthetic CT models from mri scans of the head and neck for radiation therapy," *Phys. Med. Biol.*, vol. 58, no. 23, p. 8419, 2013.

[9] J. N. H. Brunt, "Computed tomography–magnetic resonance image registration in radiotherapy treatment planning," *Clin. Oncol.*, vol. 22, no. 8, pp. 688–697, 2010.

[10] R. Geevarghese, R. O'Tuura, D. E. Lumsden, M. Samuel, and K. Ashkan, "Registration accuracy of CT/MRI fusion for localisation of deep brain stimulation electrode position: An imaging study and systematic review," *Stereotactic Funct. Neurosurg.*, vol. 94, no. 3, pp. 159–163, 2016.

[11] P. W. McLaughlin *et al.*, "The use of mutual information in registration of CT and MRI datasets post permanent implant," *Brachytherapy*, vol. 3, no. 2, pp. 61–70, 2004.

[12] R. Chuter *et al.*, "The use of deformable image registration to integrate diagnostic MRI into the radiotherapy planning pathway for head and neck cancer," *Radiotherapy Oncol.*, vol. 122, no. 2, pp. 229–235, 2017.

[13] V. Fortunati *et al.*, "Feasibility of multimodal deformable registration for head and neck tumor treatment planning," *Int. J. Radiat. Oncol. Biol. Phys.*, vol. 90, no. 1, pp. 85–93, 2014.

[14] G. J. Webster, J. E. Kilgallon, K. F. Ho, C. G. Rowbottom, N. J. Slevin, and R. I. Mackay, "A novel imaging technique for fusion of high-quality immobilised MR images of the head and neck with CT scans for radiotherapy target delineation," *Brit. J. Radiol.*, vol. 82, no. 978, pp. 497–503, 2009.

[15] G. M. Verduijn, L. W. Bartels, C. P. J. Raaijmakers, C. H. J. Terhaard, F. A. Pameijer, and C. A. van den Berg, "Magnetic resonance imaging protocol optimization for delineation of gross tumor volume in hypopharyngeal and laryngeal tumors," *Int. J. Radiat. Oncol. Biol. Phys.*, vol. 74, no. 2, pp. 630–636, 2009.

[16] A. du Bois d'Aische, M. De Craene, X. Geets, V. Grégoire, B. Macq, and S. K. Warfield, "Estimation of the deformations induced by articulated bodies: Registration of the spinal column," *Biomed. Signal Process. Control*, vol. 2, no. 1, pp. 16–24, 2007.

[17] S. Leibfarth *et al.*, "A strategy for multimodal deformable image registration to integrate PET/MR into radiotherapy treatment planning," *Acta Oncologica*, vol. 52, no. 7, pp. 1353–1359, 2013.

[18] W. E. Lorensen and H. E. Cline, "Marching cubes: A high resolution 3D surface construction algorithm," *ACM SIGGRAPH Comput. Graph.*, vol. 21, no. 4, pp. 163–169, 1987.

[19] P. J. Besl and N. D. McKay, "Method for registration of 3-D shapes," *Proc. SPIE*, vol. 1611, pp. 586–607, Apr. 1992.
[20] H. Hoppe, T. DeRose, T. Duchamp, J. McDonald, and W. Stuetzle, *Surface Reconstruction From Unorganized Points*. New York, NY, USA: ACM, vol. 26, 1992, no. 2.
[21] F. Maes, A. Collignon, D. Vandermeulen, G. Marchal, and P. Suetens, "Multimodality image registration by maximization of mutual information," *IEEE Trans. Med. Imag.*, vol. 16, no. 2, pp. 187–198, Apr. 1997.
[22] P. Viola and W. M. Wells, III, "Alignment by maximization of mutual information," *Int. J. Comput. Vis.*, vol. 24, no. 2, pp. 137–154, Sep. 1997.
[23] P. Thévenaz and M. Unser, "Optimization of mutual information for multiresolution image registration," *IEEE Trans. Image Process.*, vol. 9, no. 12, pp. 2083–2099, Dec. 2000.

QIN CHU received the B.S. degree from the Hunan University of Arts and Science, Changde, China, in 2016. She is currently pursuing the degree with the Guangdong University of Technology, Guangzhou, China. Her main research interests include computer visions and medical image processing.

YINWEI ZHAN received the B.S. degree in mathematics and the M.S. degree in computational mathematics from Jilin University, Changchun, China, in 1986 and 1988, respectively, and the Ph.D. degree in computational mathematics from the Dalian University of Technology, Dalian, China, in 1992. After being Postdoctoral Researcher with Beijing Normal University, from 1992 to 1994, he joined Shantou University, as an Associate Professor. From 2001 to 2004, he was a Postdoctoral Researcher with CWI and Groningen University, The Netherlands. He has been a Professor with the School of Computer Science and Technology, Guangdong University of Technology, Guangzhou, China, since 2015. His main research interests include computer vision, HCI, machine learning, and VR/AR applications.

FANQING GUO received the B.S. degree in applied chemistry from Fudan University, Shanghai, China, in 1991, the M.Sc. degree in radiochemistry from the Institute of High Energy Physics, Chinese Academy of Sciences, Beijing, China, in 1994, and the Ph.D. degree in nuclear chemistry from the University of California at Berkeley, Berkeley, CA, USA, in 2004. He was a Medical Physics Resident and a Postdoctoral Scholar Fellow with the University of California Davis Medical Center and the School of Medicine, Sacramento, CA, in 2007. He is currently an Assistant Professor with the Department of Therapeutic Radiology, School of Medicine, Yale University, and a Medical Physicist and a Radiological Physicist with the Department of Therapeutic Radiology, Yale-New Haven Hospital, New Haven, CT, USA. His research interests include the radiation therapy physics and radiation induced photodynamic therapy.

MENGCHUN SONG received the B.S. degree in electronic information engineering from Jiangxi Science and Technology Normal University, Nanchang, China, in 2006, and the M.S. degree in communication and information systems from Jinan University, Guangzhou, China, in 2008. He is currently a Senior Engineer with the Guangdong Medical Devices Quality surveillance and Test Institute, Guangzhou, China. His main research interests include reliability design of medical equipment, testing standard, EMC testing, and biomedical instruments.

RONGQIAN YANG received the B.S. degree in electronic instrumentation and measurement from Nanchang Hangkong University, Nanchang, China, in 2001, the M.S. degree in communication and information systems from Jinan University, Guangzhou, China, in 2005, and the Ph.D. degree in biomedical engineering from Shanghai Jiao Tong University, Shanghai, China, in 2009. He is currently an Associate Professor with the Department of Biomedical Engineering, South China University of Technology, Guangzhou, China, a Visiting Associate Professor with the Department of Therapeutic Radiology, Yale University, New Haven, CT, USA, and a Deputy Director of the Guangdong Engineering Technology Research Center for Translational Medicine of Mental Disorders. His main research interests include biomedical signal and image processing, machine vision, medical robot, and biomedical instruments.